CO-REGISTRATION OF A NEEDLE-POSITIONING DEVICE WITH A VOLUMETRIC X-RAY MICRO-COMPUTED TOMOGRAPHY SCANNER FOR IMAGE-GUIDED PRECLINICAL INTERVENTIONS

Adam C. Waspe, David W. Holdsworth, James C. Lacefield, and Aaron Fenster

Biomedical Engineering Graduate Program, and Imaging Research Laboratories,
Robarts Research Institute, University of Western Ontario, London, ON, Canada

ABSTRACT

An apparatus and method are developed for integration of a needle-positioning robot with volumetric micro-computed tomography image guidance for interventions in small animals. Accurate registration is critical for integration as it enables targets identified in the image to be mapped to physical coordinates inside the animal. Registration is accomplished by injecting barium sulfate into needle tracks created in a tissue-mimicking phantom. Registration accuracy is therefore affected by the positioning error of the robot and is assessed by measuring the point-to-line target registration error (TRE). Centroid points along cross-sectional slices of the track are determined using region growing segmentation followed by application of a center-of-mass algorithm. The centerline points are registered to needle trajectories in robot coordinates by applying an iterative closest point algorithm between points and lines. Implementation of this procedure with four fiducial needle tracks produced a point-to-line TRE of 194 ± 18 μm.

Index Terms— image-guided intervention, small animal imaging, x-ray micro-computed tomography, image registration, iterative closest point.

1. INTRODUCTION

The delivery of cells [1], therapeutics [2], or contrast agents [3] to specific targets in small-animal models of disease is often required in preclinical research protocols. In order to target small cavities and vessels in mice accurately, the needle positioning error needs to be < 200 μm [4]. If targeting is inaccurate, experimental results can be inconclusive or misleading, thus increasing the number of animals, the duration, and the cost of a study.

High-frequency ultrasound has recently been used to improve targeting during needle insertion procedures in small animals [1], [2]. Ultrasound enables visualization of the needle in real time as it is inserted into the tissue. Ultrasound reflects strongly at bony interfaces, however, and is therefore not suitable for imaging intracranial targets during stereotactic procedures [5] or for procedures that require visualizing bone landmarks, such as joint arthrography [3].

We have interfaced a robotic needle manipulator with a volumetric x-ray micro-computed tomography scanner (VCT). Registration of the two systems allows target coordinates found in an image to be mapped to the physical coordinate system of the robot. An initial 3-D image of the target and surrounding area is used to select a desired target and trajectory within the animal. The system transforms the target point and trajectory into robot coordinates and moves the needle to the target position. This technique has been used for clinical research applications, but applications to small animal research are just beginning to emerge [6], [7].

In this paper, we present the design of an intervention platform that allows a needle-positioning robot to be mechanically coupled to the VCT and provides attachments for an animal bed in imaging and intervention positions. We demonstrate the repeatability of repositioning the animal bed between imaging and intervention locations. We also evaluate a method of performing image-to-physical-space registration that employs an iterative closest point (ICP) algorithm to relate segmented contrast-enhanced needle tracks to programmed robot trajectories. The registration error of these transformations is characterized.

2. MATERIALS AND METHODS

2.1. System Description

The system consists of a custom three degree-of-freedom (DOF) needle-positioning robot and a GE eXplore Locus Ultra Pre-Clinical CT Scanner (General Electric Healthcare, London, Ontario, Canada). The design of the robot is based on a remote center of motion (RCM), which creates a fulcrum point for angulation of the needle. When the needle tip is placed directly at the RCM and on the surface of the animal, the tip can pivot about the skin entry point to allow the orientation of the needle to be manipulated without breaking the skin. The robot can translate the needle along linear trajectories from the RCM. The mean positioning error of the robot in free space is about 100 μm [4]. A photograph of the needle-positioning robot coupled to the intervention platform mounted on the VCT is shown in Fig. 1 (a).

The eXplore Ultra volumetric micro-CT scanner incorporates a digital flat-panel detector and a slip-ring gantry to enable rapid 3-D image acquisition with a transaxial field of view of 14 cm and a frame rate up to 1 Hz. A 3-D cone-beam reconstruction algorithm is employed, yielding a 150 μm isotropic voxel size. Modulation transfer function measurements from an image of a slanted edge in a quality assurance phantom indicate that the in-plane spatial resolution is 200 μm [8]. Operating the scanner with a 120 kVp tube voltage and a 20 mA tube current for a 16 s anatomical scan produces high contrast for the barium sulfate contrast agent used to enhance needle insertion paths for image-to-physical-space registration.

Financial support for this project provided by the Canadian Institutes of Health Research, the Ontario Research and Development Challenge Fund, and General Electric Healthcare Biosciences. ACW holds a PGS-D scholarship from the Natural Sciences and Engineering Research Council of Canada. DWH is a Career Investigator supported by the Heart and Stroke Foundation of Ontario. AF holds a Tier 1 Canada Research Chair in Biomedical Engineering. (email: awaspe@imaging.robarts.ca)

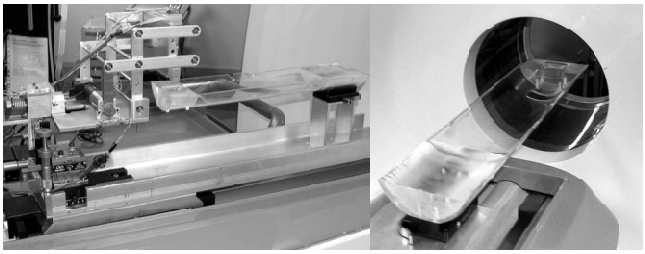

(a) (b)

Fig. 1. The needle-positioning robot coupled to the VCT with an intervention platform, with (a) the animal bed located at the intervention position, and (b) the animal bed inside the bore of the scanner.

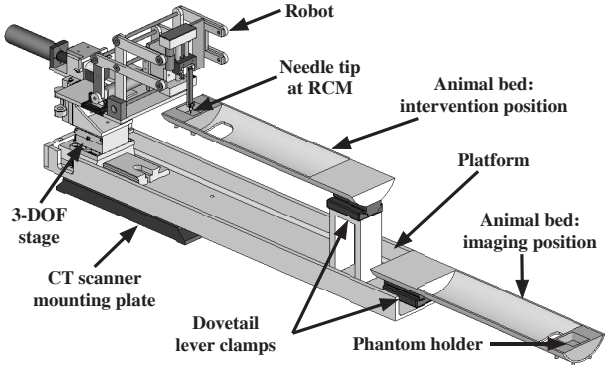

Fig. 2. A 3-D diagram of the needle-positioning robot attached to the intervention platform. The diagram shows the animal bed clamped in two positions: an imaging position, which places the region of interest at the isocenter of the scanner bore, and an intervention position, which places the region of interest in the robot workspace. The bed is secured in each location by a dovetail lever clamp.

2.2. System Integration and Registration

Since the height of the robot is 20% larger than the 25 cm bore of the VCT, the animal bed must be moved outside the bore to the robot workspace when an intervention is performed (Fig. 1). This complicates the intervention procedure because the variability in relocating the animal bed between imaging and intervention sessions needs to be controlled and minimized. The robot platform is attached to a mounting plate so that it is aligned with the animal translation stage, with the robot situated towards the back of the platform to prevent collisions with the scanner. The robot is mounted on a 3-DOF Cartesian positioning stage so that the RCM point can be aligned with the skin entry point on the animal. This changes the translation component of the transformation between the coordinate systems of the robot and the scanner, but the positioning stages are sufficiently precise that the registration would not need to be repeated if the RCM point was moved.

The animal bed locks in two positions with lever-actuated dovetail clamps, as seen in Fig. 2. In the imaging position, the region of interest is located in the center of the scanner bore, whereas in the intervention position the bed is rotated in the horizontal plane by 180° and translated so that the region of interest is in the robot workspace. The animal bed insert is modular so that the calibration phantom holder can be replaced with a stereotactic frame and ear bars or a leg restraint device.

The calibration phantom holder was filled with a gelatin tissue-mimicking phantom. A 27G, 0.5 in needle and a 1 mL syringe was attached to the robot, and the robot was calibrated as outlined by Waspe *et al.* [4]. The syringe was connected by laboratory tubing to a programmable syringe pump (model NE-1000, New Era Pump Systems, Inc., Wantagh, NY, USA) and filled with barium sulfate. The pump was programmed to dispense 40 μL of contrast agent at a rate of 90 μL/min. The dispensed volume was $\sim 40\times$ the volume of the needle track. The excess volume was required because capillary action would draw the contrast up and out of the track and the pressure required to inject into a closed hole was high.

The RCM point was positioned at the surface of the phantom so that the needle could pivot about the tissue entry point. This point was defined as the home position or origin in robot coordinates. The needle was inserted to four fiducial positions located at robot coordinates of x = $\pm$4 mm, y = $\pm$6 mm and a depth of z = 6 mm. A target position was specified at x = 0 mm, y = 0 mm and z = 6 mm. Infusion of contrast agent was initiated as the needle was retracted at a rate of 0.25 mm/s from each fiducial point and the target point, leaving a trail of contrast agent along the needle track. Any pooling of contrast agent on the surface of the phantom was removed with a cotton swab. The animal bed was moved to the imaging position and the platform was advanced into the bore of the VCT.

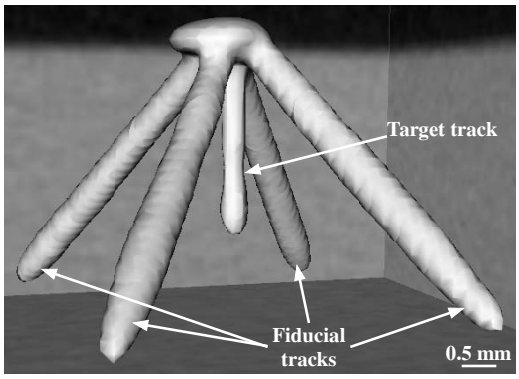

Fig. 3. An isosurface rendering of the four contrast-enhanced fiducial needle tracks and the target needle track.

Once the image was reconstructed, the individual needle tracks were segmented slice by slice using a 2-D region growing algorithm [9] followed by an intensity-weighted centroiding algorithm [10]. The centroid points from each fiducial line were coarsely fit to robot trajectories of the needle using an initial point-based rigid-body registration [11] followed by a fine-tune fit by an iterative closest point algorithm [12]. The result was used to transform the target needle track centroid points to robot coordinates for registration evaluation. A representative isosurface rendered image of the contrast-enhanced needle tracks created using MicroView (Version ABA 2.1.1, General Electric Healthcare, London, ON, Canada) is shown in Fig. 3.

2.3. Image-to-Physical-Space Registration Error

An illustrative registration result is shown in Fig. 4. Since there is not a one-to-one correspondence between needle-track centroids in the VCT image and the needle trajectory lines in robot coordinates, traditional definitions of fiducial and target registration error (FRE, TRE) are not valid. Adapting a method of calculating surface

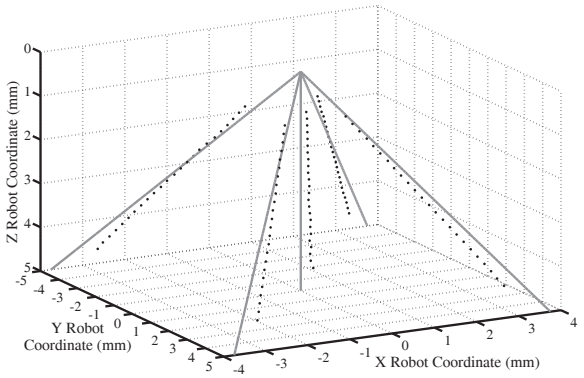

Fig. 4. Centroid points (black circles), segmented from micro-CT image data, registered to robot trajectories (gray lines). Axes are in reference to the robot coordinate system.

registration error defined by Maurer *et al.* [13], the residual error of the rigid-body registration is determined by finding the distance from each transformed centroid point to the closest point on the corresponding robot trajectory line. The perpendicular distance from each point to the corresponding line is given by:

$$\left\| perp_{\vec{d}}(\overrightarrow{AB}) \right\| = \left\| \overrightarrow{AB} - \frac{\overrightarrow{AB} \bullet \vec{d}}{\left\| \vec{d} \right\|^2} \vec{d} \right\|, \quad (1)$$

where B is a transformed centroid point, $\vec{d}$ is the direction vector of the fiducial line, and A is a point on the fiducial line.

The point-to-line FRE can then be defined as the mean and standard deviation of the minimum distance of each fiducial needle-track centroid point to the corresponding fiducial line. Likewise, the point-to-line TRE can be calculated using the points and line from the target needle track.

2.4. Stage Translation and Bed Reattachment Error

Since the platform must be translated in and out of the bore between imaging and intervention procedures, the repeatability of translating the stage was quantified. This analysis was necessary in order to determine if the transformation between robot and CT coordinates, which was found using the calibration phantom, can be applied reliably to images of an animal during subsequent interventions.

A micro-CT quality assurance phantom designed specifically for the eXplore Ultra scanner was imaged at 80 kVP and 70 mA for an 8 s anatomical scan [8]. The phantom features a geometric accuracy plate that contains five 280-μm diameter tungsten carbide spheres. Repeatedly measuring the bead locations, without moving the phantom, quantifies the error in localizing the spheres independent from the error in translating the platform. The plate was imaged five times and the centroid positions of the spheres were measured using the region growing and centroiding algorithms in MicroView and averaged. The threshold level for the segmentation was set to 30% of the peak intensity through each bead. This value was determined empirically by varying the threshold and measuring the quantized volume of the segmented bead. The Cartesian variance components of the centroid locations were used to calculate the FLE [10] as:

$$FLE = \sqrt{\sigma_x^2 + \sigma_y^2 + \sigma_z^2}, \quad (2)$$

where σ_x^2, σ_y^2, and σ_z^2 are the Cartesian variances of locating the centroid of the fiducials from repeated centroid measurements of the bead position in five micro-CT images with the phantom in a fixed position.

The platform was translated in and out of the bore four times and the phantom was imaged each time it re-entered the bore. The outer four bead centroids were used as fiducials for a rigid-body point-based registration and the central bead centroid was used as a target for evaluation. The four post-translation scans were each rigidly registered to the average centroid coordinates of the five pre-translation images using the method of Arun *et al.* [11]. The mean and standard deviation of the three rotation (α_x, β_y, γ_z) and three translation (Δ_x, Δ_y, Δ_z) terms of the 6-DOF rigid-body transformation were calculated. The fiducial registration error (FRE) was calculated as:

$$FRE = \sqrt{\frac{1}{N} \sum_{i=1}^{N} \left\| q_i - F(p_i) \right\|^2}, \quad (3)$$

where q_i are the fiducial coordinates in the target (averaged) image, p_i are the fiducial coordinates in the source (repositioned) image, N is the number of fiducials, and F is the transformation that registers the source to the target points. The target registration error (TRE) was calulated similarly by substituting the fiducial points with the target point [14].

The animal bed also has to be repositioned in the dovetail clamps between imaging and intervention procedures. The repeatability of this procedure was assessed using the same technique as was used for the translation of the intervention platform. The mean and standard deviation of the 6-DOF rigid-body transformation as well as the FRE and TRE were calculated as above.

3. RESULTS AND DISCUSSION

3.1. Image-to-Physical-Space Registration Error

The mean and standard deviation of the point-to-line FRE and TRE were 246 $\pm$ 58 μm and 194 $\pm$ 18 μm, respectively. Considering that the fiducial and target needle tracks are produced by physically moving the needle to a set of coordinates and that the robot positioning error is deterministic and is on the order of 100 μm [4], a large component of the registration error is likely due to robot positioning error. The positioning error is evident in Fig. 4, where the best fit to each set of fiducial centroid points diverge from the robot trajectory fiducial lines. Improving the robot calibration and reducing positioning error would further improve the overall registration.

The physical interaction of the needle with the gelatin-based tissue-mimicking phantom could be another source of error. Visible deformation of the phantom-surface was observed during these experiments and, given the slanted bevel design of the needle, significant needle bending or deflection not observable with the naked eye could have occurred [15]. Since the goal of this procedure is calibration and not needle targeting validation, replacing the gelatin with a less elastic material such as agar should reduce the effects of needle-tissue interaction [15].

3.2. Stage Translation and Bed Reattachment Error

The measured FLE calculated using (2) for the platform translation and bed reclamping scans were 20.5 and 10.7 μm, respectively. Since the variance components are determined from five scans without moving the phantom, the measured FLE is primarily due to pho-

Table 1. Registration error parameters for stage translation and animal bed reattachment. Errors are all reported in micrometers (μm), except angular errors, which are reported in degrees.

Error Metric	Stage Translation		Bed Reattachment	
	Mean	STD	Mean	STD
α_x ($^\circ$)	-0.007	0.012	0.001	0.004
β_y ($^\circ$)	-0.007	0.006	-0.002	0.004
γ_z ($^\circ$)	-0.038	0.081	0.009	0.032
Δ_x (μm)	-28.5	64.9	5.3	24.0
Δ_y (μm)	29.2	62.3	-8.8	22.0
Δ_z (μm)	14.5	10.9	-7.3	10.4
FRE (μm)	11.4	2.6	6.3	3.1
TRE (μm)	13.7	5.8	15.3	6.4

ton counting noise and does not include the error component due to spatial quantization [14].

Table 1 summarizes the registration error parameters for the intervention platform translation and the animal bed reattachment. For the platform translation, the translation errors are larger than the registration errors. The overall mean FRE and TRE for all repositioning procedures, calculated by adding the individual mean registration errors from the stage translation and bed reattachment in quadrature [14], were 13.0 and 19.3 μm, respectively.

For the platform translation and bed reattachment procedures, the translation repeatability (standard deviations of (Δ_x, Δ_y, Δ_z)) are larger than the overall registration errors (FRE, TRE). Performing a point-based registration between subsequent scans would therefore be more accurate than relying on the translation stage and dovetail clamps alone. Registration between subsequent scans can be accomplished by attaching fiducial beads onto the animal bed that can be used to register pre- and post-intervention images.

4. CONCLUSION

We have demonstrated a method to register a volumetric x-ray micro-computed tomography scanner to a robotic needle-positioning device. The technique registers centroid points, segmented from cross-sectional slices of contrast-enhanced needle tracks, to robot trajectories by employing an iterative closest point algorithm. The registration protocol requires manipulation of the robot end effector and therefore accounts for the intrinsic positioning error of the robot. Implementing this registration procedure by injecting four fiducial needle tracks and one target needle track produced a point-to-line target registration error of 194 $\pm$ 18 μm, which is suitable for needle targeting interventions in small animal models of disease.

5. ACKNOWLEDGMENTS

The authors thank D.D. McErlain, J. Montreuil and H.N. Nikolov for suggestions related to the design and fabrication of the intervention platform. The authors also thank A. Samani for assistance with the ICP registration algorithm and M. Bygrave and J. Umoh for micro-CT scanning assistance.

6. REFERENCES

[1] M. L. Springer, R. E. Sievers, M. N. Viswanathan, M. S. Yee, E. Foster, W. Grossman, and Y. Yeghiazarians, "Closed-chest cell injections into mouse myocardium guided by high-resolution echocardiography," *Am. J. Physiol. Heart Circ. Physiol.*, vol. 289, no. 3, pp. H1307–H1314, 2005.

[2] J. C. Slevin, L. Byers, M. Gertsenstein, D. Qu, J. Mu, N. Sunn, J. C. P. Kingdom, J. Rossant, and S. L. Adamson, "High resolution ultrasound-guided microinjection for interventional studies of early embryonic and placental development *in vivo* in mice," *BMC Dev. Biol.*, vol. 6, no. 10, pp. 1–14, 2006.

[3] F. W. Roemer, A. Mohr, J. A. Lynch, M. D. Meta, A. Guermazi, and H. K. Genant, "Micro-CT arthrography: a pilot study for the *ex vivo* visualization of the rat knee joint," *Am. J. Roentgenol.*, vol. 184, no. 4, pp. 1215–1219, 2005.

[4] A. C. Waspe, H. J. Cakiroglu, J. C. Lacefield, and A. Fenster, "Design, calibration and evaluation of a robotic needle-positioning system for small animal imaging applications," *Phys. Med. Biol.*, vol. 52, no. 7, pp. 1863–1878, 2007.

[5] E. Chan, N. Kovacevíc, S. K. Ho, R. M. Henkelman, and J. T. Henderson, "Development of a high resolution three-dimensional surgical atlas of the murine head for strains 129S1/SvImJ and C57Bl/6J using magnetic resonance imaging and micro-computed tomography," *Neuroscience*, vol. 144, no. 2, pp. 604–615, 2007.

[6] P. Kazanzides, J. Chang, I. Iordachita, J. C. Li, C. C. Ling, and G. Fichtinger, "Development of an image-guided robot for small animal research," *Comput. Aided Surg.*, vol. 12, no. 6, pp. 357–365, 2007.

[7] A. C. Waspe, J. C. Lacefield, and A. Fenster, "Registration of three-dimensional high-frequency ultrasound images to a robotic needle-positioning system for pre-clinical research," in *Proc. 4th IEEE ISBI*, 2007, pp. 1132–1135.

[8] L. Y. Du, J. Umoh, H. N. Nikolov, S. I. Pollmann, T. Y. Lee, and D. W. Holdsworth, "A quality assurance phantom for the performance evaluation of volumetric micro-CT systems," *Phys. Med. Biol.*, vol. 52, no. 23, pp. 7087–7108, 2007.

[9] R. C. Gonzalez, R. E. Woods, and S. L. Eddins, *Digital Image Processing Using MATLAB*, Prentice-Hall Inc., Upper Saddle River, NJ, 2004.

[10] M. Y. Wang, C. R. Maurer, Jr., J. M. Fitzpatrick, and R. J. Maciunas, "An automatic technique for finding and localizing externally attached markers in CT and MR volume images of the head," *IEEE Trans. Biomed. Eng.*, vol. 43, no. 6, pp. 627–637, 1996.

[11] K. S. Arun, T. S. Huang, and S. D. Blostein, "Least-squares fitting of two 3-D point sets," *IEEE Trans. Pattern Anal. Mach. Intell.*, vol. 9, no. 5, pp. 698–700, 1987.

[12] P. J. Besl and N. D. McKay, "A method for registration of 3-D shapes," *IEEE Trans. Pattern Anal. Mach. Intell.*, vol. 14, no. 2, pp. 239–256, 1992.

[13] C. R. Maurer, Jr., G. B. Aboutanos, B. M. Dawant, R. J. Maciunas, and J. M. Fitzpatrick, "Registration of 3-D images using weighted geometrical features," *IEEE Trans. Med. Imaging*, vol. 15, no. 6, pp. 836–849, 1996.

[14] C. R. Maurer, Jr., J. M. Fitzpatrick, M. Y. Wang, R. L. Galloway, Jr., R. J. Maciunas, and G. S. Allen, "Registration of head volume images using implantable fiducial markers," *IEEE Trans. Med. Imaging*, vol. 16, no. 4, pp. 447–462, 1997.

[15] G. Wan, Z. Wei, L. Gardi, D. B. Downey, and A. Fenster, "Brachytherapy needle deflection evaluation and correction," *Med. Phys.*, vol. 32, no. 4, pp. 902–909, 2005.